의학박사 학위논문

Induction of the *BRAF*^{V600E} Mutation in Thyroid Cells Leads to Frequent Hypermethylation

갑상선 세포주에 유도된 *BRAF*^{V600E} 돌연변이에 의한 메틸화 변화

2023 년 2 월

서울대학교 대학원

의학과 외과학 전공

이 진 욱

갑상선 세포주에 유도된 *BRAF*^{V600E} 돌연변이에 의한 메틸화 변화

지도교수 이 규 언

이 논문을 의학박사 학위논문으로 제출함

2022 년 10월

서울대학교 대학원

의학과 외과학 전공

이 진 욱

이진욱의 의학박사 학위논문을 인준함

2023년 1월

위 원 장 _____ (인)

부 위 원 장 _____ (인)

위 원 _____ (인)

위 원 _____ (인)

위 원 _____ (인)

Induction of the *BRAF*^{V600E} Mutation in Thyroid Cells Leads to Frequent Hypermethylation

by Jin Wook Yi, M.D.

(Directed by Kyu Eun Lee, M.D., Ph.D.)

A Thesis Submitted to the Department of Surgery in Partial Fulfilment of the Requirements for the Degree of Doctor of Philosophy in Medicine (Surgery) at Seoul National University College of Medicine, Seoul, Korea

January 2023

Approved by thesis committee

Professor _____ Chairman

Professor _____ Vice Chairman

Professor _____

Professor _____

Professor _____

Abstract

Induction of the *BRAF*^{V600E} Mutation in Thyroid Cells Leads to Frequent Hypermethylation

Jin Wook Yi

Medicine (Surgery)

The Graduate School

Seoul National University

Background:

The *BRAF*^{V600E} mutation is a major driver mutation in papillary thyroid cancer. The aim of this study was to elucidate the correlation between DNA methylation and gene expression changes induced by the *BRAF*^{V600E} mutation in thyroid cells.

Methods:

I used Nthy/BRAF cell lines generated by transfection of Nthy/ori cells with the wild-type *BRAF* gene (Nthy/WT cells) and the V600E mutant-type *BRAF* gene (Nthy/V600E cells). I performed gene expression microarray and DNA methylation array analyses for Nthy/WT and Nthy/V600E cells. Two types of array data were integrated to identify inverse correlations between methylation and gene expression. The results were verified in silico using data from The Cancer Genome Atlas (TCGA) and in vivo through pyrosequencing and quantitative real-time polymerase chain reaction (qRT-PCR).

Results:

In the Nthy/V600E cells, 199,821 probes were significantly hypermethylated, and 697 genes showed a “hypermethylation–downregulation” pattern in Nthy/V600E. Tumor suppressor genes and apoptosis–related genes were included. In total, 66,446 probes were significantly hypomethylated, and 227 genes showed a “hypomethylation–upregulation” pattern in Nthy/V600E cells. Protooncogenes and developmental protein–coding genes were included. In the TCGA analysis, 491/697 (70.44%) genes showed a hypermethylation–downregulation pattern, and 153/227 (67.40%) genes showed a hypomethylation–upregulation pattern. Ten selected genes showed a similar methylation–gene expression pattern in pyrosequencing and qRT–PCR.

Conclusions:

Induction of the *BRAF*^{V600E} mutation in thyroid cells led to frequent hypermethylation. Anticancer genes, such as those involved in tumor

suppression or apoptosis, were downregulated by upstream hypermethylation, whereas carcinogenic genes, such as protooncogenes, were upregulated by hypomethylation. Our results suggest that the *BRAF*^{V600E} mutation in thyroid cells modulates DNA methylation and results in cancer-related gene expression.

-

Keywords: Thyroid neoplasm, methylation, gene expression

Student number: 2016 – 36691

Contents

List of Tables and Figures

showed hypomethylation and upregulation in Nthy/V600E cells.

Figure 5. Possible carcinogenic mechanisms of the *BRAF*^{V600E} mutation

I. Introduction

Thyroid cancer is one of the most common solid organ cancers, and its incidence has increased dramatically in the last decade [1,2]. Papillary thyroid carcinoma (PTC) is the most common histologic subtype and is associated with the *BRAF*^{V600E} somatic mutation (Substitution of a valine by a glutamate at reside 600), which is known to be associated with poor prognostic factors such as lymph node metastasis, extrathyroidal extension, and advanced stage [3,4]. Recent report suggested that increased incidence of *BRAF*^{V600E} mutation is identified with increasing the thyroid cancer incidence [5].

The *BRAF*^{V600E} mutation is the highest signal activator of the mitogen-associated protein kinase (MAPK)/extracellular signal-regulated kinase (ERK) pathway. It activates a carcinogenic signal cascade in thyroid cells and makes them more proliferative [3]. Recent whole-genome sequencing performed by The Cancer Genome Atlas (TCGA) project further revealed that *BRAF*^{V600E} mutant-type PTC showed significant upregulation of the pERK-DUSP (Erk transcriptional program) pathway, possibly due to the insensitivity of *BRAF*^{V600E} to ERK inhibition feedback [6].

The molecular mechanism of gene expression alterations resulting from the *BRAF*^{V600E} driver mutation have not yet been fully understood. Beyond the genomic transcription, epigenomic changes, such as DNA methylation, histone modification and microRNAs can act as important factors that modulate gene expressions without the changing of DNA structure [7]. Among them, DNA methylation is special phenomenon that attach the methyl (−CH) group to the 5th carbon in Cytosine. It occurs in the repeated sequence area of C following G (CpG island) and frequently found in the upstream area from the exon (Promotor site) in DNA sequence. DNA hypermethylation or hypomethylation in the CpG island can change downstream gene expression into down− or up−regulation like a genomic switch. It is known that DNA methylation always occurred prior to the corresponding gene expression change, and DNA methylation can be changed by environmental factors surrounding organism [8].

Therefore, it can be hypothesized that when *BRAF*^{V600E} mutation occur in thyroid cells, DNA methylation may be altered by the *BRAF*^{V600E} signal activation, resulting in changes in downstream

gene expression. In thyroid cancer, prior laboratory studies have suggested that specific aberrant DNA methylation is found in cancer-related genes such as *PTEN* and *RASSF1A* [7,9]. According to advancement of next generation sequencing, genome-wide integrated analyses of methylation and expression array or sequencing from the thyroid cancer tissue or thyroid cancer cell lines are also reported elsewhere [10-17]. However, previous studies could not determine the actual consequence of primal $BRAF^{V600E}$ mutation, because cancer cell lines which used in previous studies are closed to dedifferentiated thyroid cancers such as anaplastic or already been changed into thyroid cancer [18].

Our aim of study is to investigate subsequent change of DNA methylation and gene expression in thyroid cell, initiated by primal $BRAF^{V600E}$ mutation. I used special "Nthy/BRAF" cell line – transfected BRAF gene either wild type BRAF (Nthy/WT) and mutant type BRAF (Nthy/V600E) into Nthy/ori cells, which was developed by authors' institution [19]. I performed both gene expression microarrays and methylation microarrays, and performed integrated analysis for two types of data to find the correlation between DNA

methylation with gene expression, induced by *BRAF*^{V600E} mutation in normal thyroid cells.

II. Materials and Methods

Nthy/BRAF cell line and gene expression microarray

I used previously reported Nthy/ori cell lines expressing the *BRAF* gene with or without V600E mutation [19]. Two types of Nthy/BRAF cells were presented: Nthy/WT (Nthy cells with wild-type *BRAF* gene) and Nthy/V600E (Nthy cells with V600E mutant-type *BRAF* gene). Cells were grown in RPMI-1640 (Biowest, Riverside, MO, USA) supplemented with 10% FBS (Biowest),

2 mM GlutaMAX (Gibco; Thermo Fisher Scientific, Waltham, MA, USA), and 100 U/mL penicillin-streptomycin (Gibco) in a humidified atmosphere of 5% CO2 at 37°C. They were cultured in 100-mm dishes until confluent monolayers were reached, and RNA was extracted using an easy-spin total RNA extraction kit (iNtRON Biotechnology, Seoul, Korea). Total RNA was quantified using a Nanodrop ND-1000 spectrophotometer. The Illumina HumanHT-12 v4 Expression Bead Chip (Illumina Inc., San Diego, CA, USA) microarray services were provided by Macrogen (Macrogen Inc., Seoul, Korea). Two arrays were conducted for each cell type

(2xNthy/WT and 2xNthy/V600E).

Methylation microarray

For DNA extraction, Nthy/WT and Nthy/V600E cells were cultured until a confluent monolayer was formed. Cells were harvested by trypsin–EDTA treatment, and DNA was extracted using QIAamp DNA Mini Kit (Qiagen, Hilden, Germany). DNA concentration was quantified using a spectrophotometer (NanoDrop, Wilmington, DE, USA). After DNA extraction, methylation microarray services were provided by Macrogen (Macrogen Inc., Seoul, Korea) using Illumina Infinium Methylation EPIC Bead Chip Kits (850K; Illumina Inc., San Diego, CA, USA). Three arrays were conducted for each cell type (3xNthy/WT and 3xNthy/V600E).

Bioinformatic analysis

Microarray data were analyzed according to two groups: Nthy/WT and Nthy/V600E. Raw data derived from the Illumina Genome Studio

version 2011.1 and Gene Expression Module version 1.9.0 were transformed into a "LumiBatch" object using “Lumi R package”. Variance stabilization of gene expression counts was performed using the variance-stabilizing transformation (VST) method. Quantile normalization method was applied to gene expression data after VST. Packages “Annotate" and “IlluminaHumanv4.db” were used for microarray chip probe annotation, provided by Bioconductor (http://www.bioconductor.org). To find differentially expressed genes (DEGs), moderated *t*-test using the “Limma” was applied [20]. The Benjamini-Hochberg (BH) method was applied to correct false positive rate from multiple comparisons. A log fold change value of 2 was used as the cutoff to identify significant DEGs.

Methylation array data were analyzed by “ChAMP” package provided by Bioconductor [21]. Data preparation was followed by the raw data loading, quality control, normalization, and variation control by singular value decomposition (SVD). From the filtered data, “limma” method was also applied to identify differentially methylated probes (DMPs) [20]. False positive rate correction was performed with the BH method. Adjusted *p*-value under 0.05 was considered statistically

significant for both gene expression and methylation analysis.

Genes with inverse methylation–expression patterns were identified according to the following criteria: differentially hypermethylated probes in the promoter region with downregulated gene expression or promoter region hypomethylation with upregulated gene expression, as illustrated on figure 1. The promoter region was defined as CpG islands in TSS1500, TSS200, the 5′–untranslated region (UTR) and the 1st exon area.

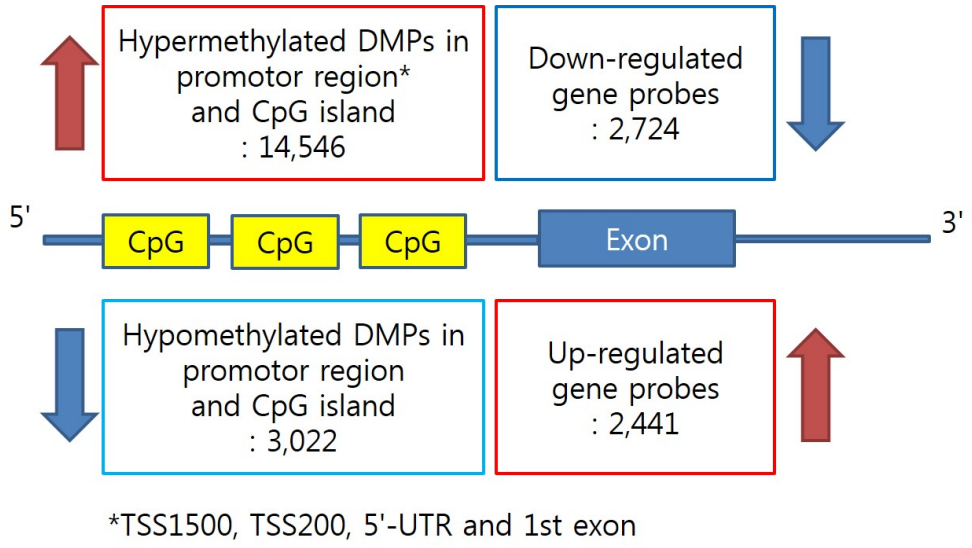

Figure 1. Schematic diagram of the correlation analysis between differentially methylated probes (DMPs) in promoters and differentially expressed genes in exons. UTR, untranslated region.

To find functional terms of inversely correlated genes, Database for Annotation, Visualization, and Integrated Discovery (DAVID 6.7) and Swiss-Prot Protein Information Resource (SP-PIR) were used [22,23]. Adjusted p-value less than 0.1 was considered statistically significant in functional analysis. All statistical analyses were performed with the R programming language (https://www.R-project.org/).

Validation of inverse correlations using a dataset from TCGA

To validate genes with inverse-correlation patterns using other public databases, I assessed somatic mutations, mRNA expression by RNA sequencing and DNA methylation by Illumina Infinium Methylation 450K from the TCGA data (https://gdc.cancer.gov/).

Patients in the TCGA cohort were divided into two groups according to *BRAF* mutation status: *BRAF* wild-type PTC versus *BRAF* mutant-type PTC. From the methylation data, only selected the methylation status from the CpG island in promotor area (TSS1500, TSS200 and other promotor region). mRNA expression

was extracted from the normalized gene expression results. Inverse correlation was detected by the Spearman correlation analysis between the methylation and gene expression value. If the same hypermethylation-downregulation or hypomethylation-upregulation pattern was observed, it was marked as "TRUE"; otherwise, it was marked as "FALSE."

Validation of gene expression by quantitative real-time polymerase chain reaction (qRT-PCR)

Nthy/WT and Nthy/V600E were grown in RPMI-1640 (Biowest) supplemented with 10% FBS (Biowest), 2mM GlutaMAXTM (Gibco), and 100U/ml penicillin-streptomycin (Gibco) in humidified atmosphere of 5% CO2 at 37℃. Cells were cultured in 100-mm dishes until confluent monolayers were formed, and total RNA was extracted using RNeasy Mini Kit (Qiagen) and quantified using Nanodrop One (Thermo Fisher). cDNA was transcribed from 1 μg of RNA using Legene Premium Express 1st strand DNA Synthesis System Kit (LeGene Biosciences, San Diego, CA, USA). Quantitative

real-time polymerase chain reaction (qRT-PCR) was performed using PowerTrack SYBR green master mix (Applied Biosystems, Waltham, MA, USA) and a QuantStudio 3 real-time PCR System (Applied Biosystems); all samples were run on the same 96-well plate. Relative mRNA expression levels were calculated by normalizing the value for each gene to that of the housekeeping gene ACTB (beta-actin). The primer sequences for qRT-PCR are described in table 1.

Table 1. Sequences of primers used for quantitative real-time polymerase chain reaction.

Gene	NCBI Reference	Forward Primer (5' -> 3')	Reverse Primer (5' -> 3')
b-Actin	NM_001101.5	GGACTTCGAGCAAGAGATGG	AGCACTGTGTTGGCGTACAG
PTEN	NM_000314.8	ACCAGGACCAGAGGAAACCT	GCTAGCCTCTGGATTTGACG
RUNX3	NM_001031680.2	CAGAAGCTGGAGGACCAGAC	TCGGAGAATGGGTTCAGTTC
MEST	NM_002402.4	CGCAGGATCAACCTTCTTTC	CATCAGTCGTGTGAGGATGG
TP53INP1	NM_033285.4	GGCCCACGTACAATGACTCT	CTGGTTCTTGGTTGGAGGAA
RASSF4	NM_032023.4	GCAAGTGGCTCAGAAAAAGG	CCCACAGGAACCAGTAGGAA
GPX3	NM_002084.5	TGCAACCAATTTGGAAAACA	TTCATGGGTTCCCAGAAGAG
CCND1	NM_053056.3	GAGGAAGAGGAGGAGGAGGA	GAGATGGAAGGGGGAAAGAG
BCL2	NM_000633.3	GGATGCCTTTGTGGAACTGT	AGCCTGCAGCTTTGTTTCAT
DUSP6	NM_001946.4	ATGGTAGTCCGCTGTCCAAC	AATGGCCTCAGGGAAAAACT
EGFR	NM_005228.5	AGGTTGTAAGGGGGAGCACT	CCAGTGCCTTTCCTGCTAAG
ZEB1	NM_001128128.3	TGCACTGAGTGTGGAAAAGC	TGGTGATGCTGAAAGAGACG

Validation of promoter methylation status by pyrosequencing

Nthy/WT and Nthy/V600E cells were cultured until confluent monolayers were formed. Genomic DNA was extracted using QIAamp DNA mini kit (Qiagen) according to manufacturer's recommendations. The genomic DNA (gDNA) concentration was quantified using a Nanodrop One (Thermo Fisher), and >1 μg/20 μL of gDNA was provided for pyrosequencing analysis.

Pyrosequencing was performed by Macrogen (Seoul, Korea) using PyroMark Q48 Autoptrep (Qiagen) system. Primers for pyrosequencing are described in table 2. EpiTect Fast DNA Bisulfite Kit (QIAGEN) was used for bisulfite treatment. The methylation rate was compared between the two types of pyrosequencing data before and after bisulfite treatment. For plotting the pyrosequencing and qRT-PCR validation results, GraphPad Prism ver. 9.1.0 for Windows (GraphPad, San Diego, CA, USA) was used.

Table 2. Primer design for pyrosequencing

Gene	Target Location	Forward Primer	Reverse Primer
RUNX3	cg13461622 :chr1: 25291385-25291385	AGGAAAGTAAGTTTTTGTTTGTATTTAAG	AACTCCTCCACCCTAACT
MEST	cg14088957 :chr7: 130131085-130131085	AGAATAGTGGGTATAATTAGGAGAGT	AATTAAAAAAAATTCCTCCCTCTTTCT
TP53INP1	cg16049864 :chr8: 95962084-95962084	GAGGGTTTGGGGTATAAAGG	TCCCAACACCCTAACTACAC
RASSF4	cg02841844 :chr10: 45455421-45455421	GTTGGAGGGGGAGGGATTT	TCCCCTCCCACCCAAAACTACCAC
GPX3	cg14237894 :chr5: 150400040-150400040	GGTGGGGAGTTGAGGGTAA	CCCAACCACCTTTCAAAC
CCND1	cg24387864 :chr11: 69454823-69454823	GGTTTTGTTGGGGGTGTAG	ATAATATTAAAAACCCTCTCATATAACC
BCL2	cg16445842 :chr18: 60986860-60986860	AGAGGGGAAGATGAAGGAGT	TCCTACCTTCATTTATCCAACAACTTT
DUSP6	cg20143530 :chr12: 89747082-89747082	GTTTGGTTGTGTAGAAAATTAGAAGAA	ATTCCCCCCAACAATAACTTATAACTCC
EGFR	cg03860890 : chr7: 55086288-55086288	TAGTGTTGTAGGGGAGGT	TCCCCCTTTCCCTTCTTTTAT
ZEB1	cg00520933 :chr10 :31607160-31607160	TAGGTGGTAGGATTTAGAGTTAAGG	ATCTTTTCAAAAATCCCAAAACTTATAC

Ethical statement

This is not the study that deals with human or animal subjects, so it doesn't need to gain the approval from Institutional Review Board/Institutional Animal Care and Use Committee (IACUC).

III. Results

Gene Expression Microarray

In total, 5,165 genes were differentially expressed between Nthy/WT and Nthy/BRAF cells. Number of up-regulated DEGs in Nthy/V600E were 2,441 and down-regulated DEGs were 2,724 (Figure 2) [19].

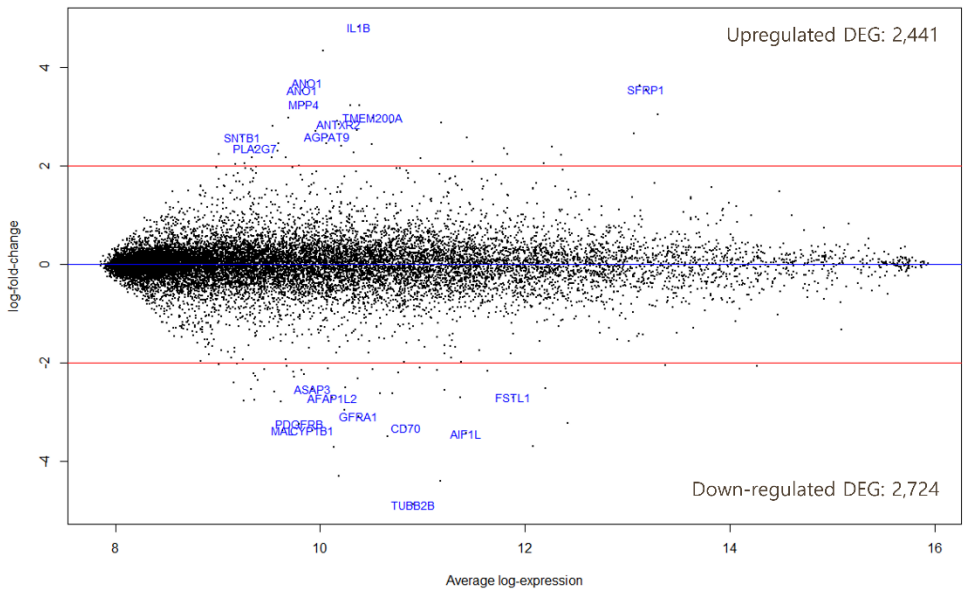

Figure 2. Microarray (MA) plot for the DEGs in the Nthy/V600E cells.

Methylation Microarray

In the methylation array analysis, total of 266,267 probes were differentially methylated between the Nthy/WT and Nthy/V600E cells. The detailed number of DMPs according to the genomic structure and geographic region of the CpG island is shown in Figure 3. Based on the side of Nthy/V600E cells, total of 199,821 probes were hypermethylated whereas 66,446 probes were hypomethylated (Figure 1).

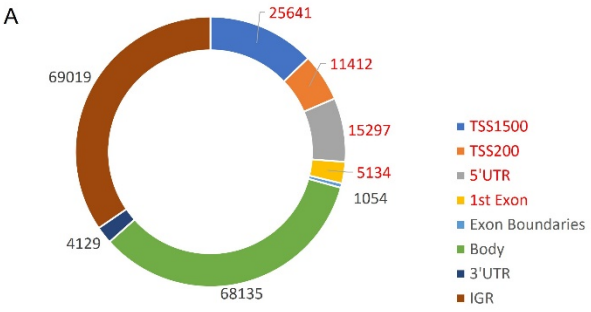
A
25641
11412
15297
5134
1054
68135
4129
69019
TSS1500
TSS200
5'UTR
1st Exon
Exon Boundaries
Body
3'UTR
IGR

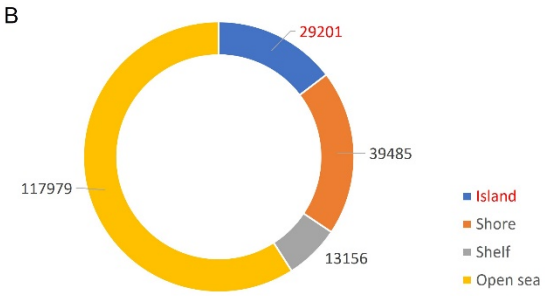
B
29201
39485
13156
117979
Island
Shore
Shelf
Open sea

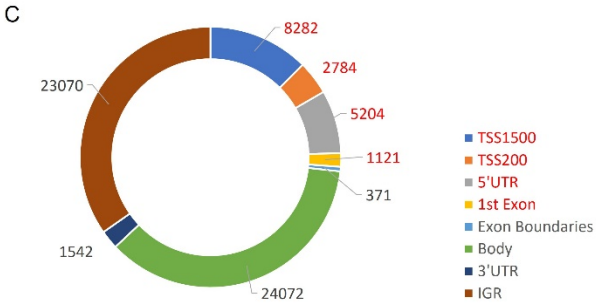
C
8282
2784
5204
1121
371
24072
1542
23070
TSS1500
TSS200
5'UTR
1st Exon
Exon Boundaries
Body
3'UTR
IGR

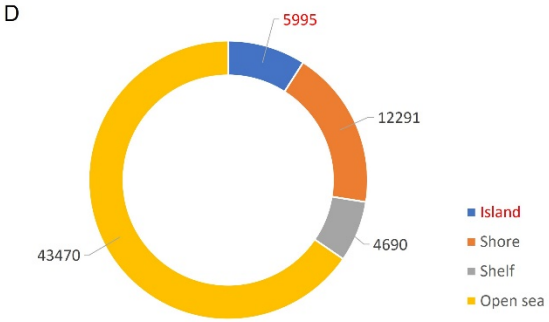
D
5995
12291
4690
43470
Island
Shore
Shelf
Open sea

Figure 3. Distribution of differentially methylated probes according to genomic location and CpG site. (A) Number of hypermethylated probes in Nthy/V600E cells; genomic structure. (B) Number of hypermethylated probes in Nthy/V600E cells; geographic regions from the CpG area. (C) Number of hypomethylated probes in Nthy/V600E cells; genomic structure. (D) Number of hypomethylated probes in Nthy/V600E cells; geographic regions from the CpG area. UTR, untranslated region; IGR, intergenic region.

Integrated Analysis of Microarrays

In the Nthy/V600E cells, number of hypermethylated DMPs in promotor region with CpG island were 14,516. Number of significantly down-regulated genes in Nthy/V600E cells were 2,724. According to genomic location, total 697 genes showed the inverse correlation pattern (Promoter hypermethylation with exonic down-regulation) in Nthy/V600E cells. Table 3 lists the top 20 genes that showed promoter hypermethylation and gene down-regulation, sorted by the number of hypermethylated probes of CpG islands in the promoter region. Apoptosis-related genes (*FASKT*, *PTEN*, *EPB41L3*), structural constituent-related genes (*FBLN2*), DNA repair genes (*MAD2L2*), and scavenger receptor genes (*SCARF2*) were included.

Table 3. Top 20 genes with DNA hypermethylation above the exonic area and downregulation of exons in Nthy/V600E cells

Gene name	Number of upstream hypermethylated probes	log FC	t-value	Adjusted p-value	Selected gene function from gene ontology database
SGCE	22	-0.872	-11.014	0.002	Calcium ion binding, cytoskeleton, cytoplasm
EPB41L3	15	-1.364	-19.244	0.001	Cell-cell junction, apoptotic process, regulation of cell shape
FASTK	12	-0.658	-5.482	0.017	Serine/threonine kinase activity, apoptotic signaling pathway
DPYSL4	11	-1.232	-15.216	0.001	Pyrimidine nucleobase catabolic process, axon guidance
PTEN	11	-0.495	-6.981	0.009	Apoptotic process, epidermal growth factor

					signaling pathway
KIAA1217	10	-1.020	-10.900	0.003	Cytoplasm Embryonic skeletal system development
NTF3	10	-0.398	-6.606	0.010	Activation of MAPK activity
FAM163A	10	-0.344	-5.730	0.015	Integral to membrane
PAOX	9	-1.329	-14.875	0.001	Cellular nitrogen compound metabolic process
RUNX3	9	-0.902	-11.945	0.002	Negative regulation of transcription and cell cycle
ZFP3	9	-0.392	-6.522	0.010	DNA-templated, regulation of transcription
PRMT6	9	-0.335	-4.078	0.040	Histone methylation, negative regulation of transcription

UNC45A	9	-0.294	-4.076	0.040	Cell differentiation, perinuclear region of cytoplasm
MEST	9	-0.250	-4.026	0.041	Endoplasmic reticulum, regulation of lipid storage
CYP24A1	8	-1.604	-4.462	0.031	Vitamin D receptor signaling pathway
FAM110A	8	-0.539	-8.772	0.005	Cytoplasm, microtubule organizing center
FBLN2	8	-0.466	-4.293	0.035	Extracellular matrix structural constituent
SAMD11	8	-0.397	-4.283	0.035	Negative regulation of transcription from RNA polymerase II
MAD2L2	8	-0.317	-4.440	0.031	Negative regulation of transcription, DNA repair

SCARF2	7	-1.081	-15.262	0.001	Scavenger receptor activity

Conversely, the number of hypomethylated DMPs in the promoter region in Nthy/V600E cells was 3,022, and 2,441 genes were significantly upregulated. Total 227 genes had inverse correlation pattern of promoter hypomethylation and exon up-regulation in Nthy/V600E cells. Table 4 shows the top 20 genes that have the DNA hypomethylation and exon up-regulation in Nthy/V600E cells. Cell cycle-related genes (*CCND1*, *BCL2*, *PSMD5*), MAPK activation-related genes (*GHR*), and transmembrane transporter-related genes (*SLC6A15*, *BCL2*, *HOXB7*, *NPAS2*, *KCNK1*, *ARHGAP22*) were included.

Table 4. Top 20 genes that had an inverse correlation with hypomethylation and upregulation in Nthy/V600E cells

Gene name	Number of upstream hypomethylated probes	log FC	t-value	Adjusted p-value	Selected gene function from gene ontology database
CCND1	8	1.184	11.630	0.002	Mitotic cell cycle, positive regulation of protein phosphorylation
THBD	7	0.570	9.215	0.004	Negative regulation of platelet activation, leukocyte migration
NTNG1	6	0.594	7.708	0.007	Axonogenesis,anchored to plasma membrane
NPAS2	5	2.031	24.169	0.000	DNA binding transcription factor, signal transducer
SLC6A15	5	0.961	8.960	0.004	Proline:sodium symporter activity,

					neurotransmitter transporter
HOXB7	5	0.667	10.938	0.003	Sequence-specific DNA binding transcription factor activity
BCL2	5	0.666	11.088	0.002	G1/S transition of mitotic cell cycle, negative regulation of apoptotic process and mitotic cell cycle
TMEM108	5	0.439	7.422	0.007	Integral to membrane
SPRY4	4	2.731	18.910	0.001	Negative regulation of MAP kinase activity
SATB2	4	1.690	20.881	0.001	Negative regulation of transcription from RNA polymerase II
GAD1	4	1.259	14.122	0.001	Glutamate decarboxylation to succinate

KCNK1	4	1.077	16.265	0.001	Potassium ion transport,synaptic transmission
GHR	4	0.939	15.545	0.001	Activation of MAPK activity, activation of JAK2 kinase activity
ARHGAP22	4	0.897	9.592	0.004	Regulation of small GTPase mediated signal transduction
PSMD5	4	0.705	11.726	0.002	Signal transduction by p53 class mediator resulting in cell cycle arrest
SLAIN1	4	0.681	7.139	0.008	NA
HAS3	4	0.525	4.934	0.023	Positive regulation of transcription, hyaluronan biosynthetic process
RIPPLY2	4	0.435	6.315	0.011	Ossification, somitogenesis

MRPS14	4	0.295	4.582	0.029	Structural constituent of ribosome, mitochondrion
CPEB1	4	0.264	4.027	0.041	Cytoplasmic mRNA processing

Data Based Functional Analysis

SP-PIR keywords obtained from 697 hypermethylated-downregulated genes in Nthy/V600E are listed in Table 5. Tumor suppressor genes (*RASSF4, PRR5, PLA2G16, CADM1, EFNA1, PYCARD, BIN1, MN1, PTEN*, *MTUS1*) were downregulated in response to upstream hypermethylation in Nthy/V600E cells. Table 6 lists the SP-PIR terms corresponding to the 227 hypomethylated-upregulated genes in Nthy/V600E cells. Protooncogenes (*EGFR, FGF5, CCND1, FLI1, MAFB, BCL2, ETV1, FOXO1, MECOM, CBFB*) were upregulated in response to upstream hypomethylation in Nthy/V600E cells.

Table 5. SP-PIR keywords obtained from 697 hypermethylated-downregulated genes in Nthy/V600E cells

Term	P-value	Fold enrichment	Genes
Glyoxylate bypass	0.069	28.370	*IDH2, IDH1*
Stress-induced protein	0.030	10.639	*STK25, HSPB1, SERPINH1*
Ehlers-Danlos syndrome	0.055	7.737	*COL1A1, B4GALT7, ADAMTS2*
Cholesterol biosynthesis	0.004	7.466	*CYB5R3, TM7SF2, HMGCR, CYP51A1, FDFT1*
Sterol biosynthesis	0.011	5.674	*CYB5R3, TM7SF2, HMGCR, CYP51A1, FDFT1*
Tyrosine-specific phosphatase	0.004	5.491	*PTPRM, PTPRE, PTPN2, PTPRA, PTPRN, CDC25B*
Dwarfism	0.010	4.480	*COL9A2, FGFR3, PTH1R, DYM, COL1A1, FLNB*

Steroid biosynthesis	0.013	4.256	*CYB5R3, TM7SF2, HMGCR, CYP51A1, ACAT2, FDFT1*
Homotetramer	0.087	3.783	*ASS1, GUSB, ALDH2, FUCA1*
Triple helix	0.094	3.661	*COL9A2, COL6A1, COL1A1, COL16A1*
Hydroxylysine	0.094	3.661	*COL9A2, COL6A1, COL1A1, COL16A1*
Phospholipid biosynthesis	0.059	3.377	*CHKA, CPT1B, ISYNA1, CRLS1, ETNK2*
Fatty acid biosynthesis	0.064	3.299	*PTGIS, SCD, ELOVL2, FADS3, FADS2*
Phosphoric monoester hydrolase	0.011	3.289	*PTPRM, PTPRE, PTPN2, PTPRA, PGAM1, PPP3CC, PTPRN, CDC25B*
Lipid synthesis	0.002	3.184	*CYB5R3, TM7SF2, A4GALT, PTGIS, HMGCR, CYP51A1, SCD, ELOVL2, FADS3, FADS2, FDFT1*

Copper	0.050	2.986	*ATOX1, COX17, MT1X, MOXD1, APLP1, MT1F*
Tyrosine-specific protein kinase	0.088	2.955	*DDR1, FGFR4, FGFR3, ERBB2, ROR2*
LIM domain	0.039	2.797	*LIMS2, LMO1, PRICKLE1, LIMK2, PDLIM1, ISL1, TES*
Collagen	0.019	2.688	*CTHRC1, COL9A2, C1QL1, COL6A1, SCARA3, COL1A1, C1QL4, COL16A1, WDR33*
GTP binding	0.087	2.541	*RAB31, TUBB2B, GNB2, GNAI1, TUBB2A, RHEB*
Heterodimer	0.029	2.479	*INHBB, HLA-H, TUBB2B, TUBB2A, ITGB4, TUBA4A, PPP3CC, HLA-B, ADD3*
Blocked amino end	0.043	2.467	*SRI, CYB5R3, PFN1, GSTM3, SERPINB6, GNAI1, CSTB, COL6A1*
Growth factor	0.017	2.382	*INHBB, VEGFB, FGF18, PDGFB, NTF3, GDF6, NRG1,*

			GDF15, VGF, MDK, NGF
Tyrosine-protein kinase	0.042	2.300	*DDR1, FGFR4, FGFR3, CLK3, ERBB3, ERBB2, TESK1, ROR2, EPHB4*
Prenylation	0.022	2.182	*RND2, PALM, RAB31, PRICKLE1, MRAS, RHEB, RAB15, RAB6B, RHOD, RAB20, RASD2, GNG7*
Protein phosphatase	0.040	2.182	*MTMR3, DUSP18, PTPRM, PPM1E, PTPRE, PTPN2, PTPRA, PPP3CC, PTEN, CDC25B*
Tumor suppressor	0.053	2.071	*RASSF4, PRR5, PLA2G16, CADM1, EFNA1, PYCARD, BIN1, MN1, PTEN, MTUS1*
Actin-binding	0.007	2.067	*MYO1C, HIP1R, SPIRE1, TMSB10, MTSS1L, PALLD, TPM2, TPM1, FLNB, DSTN, PFN1, EPB41L3, CORO1A, AIF1L,*

			ADD3, FHOD1, ADD1, SNTA1
NADP	0.049	2.000	*BLVRA, ME1, TM7SF2, CYP24A1, HMGCR, CYP51A1, IDH2, IDH1, NADK, HSD11B1L, FDFT1*

SP-PIR, Swiss-Prot Protein Information Resource.

Table 6. SP-PIR keywords from 227 hypomethylated-upregulated genes in Nthy/V600E cells

Term	P-Value	Fold Enrichment	Genes
Proto-oncogene	0.001	3.767	*EGFR, FGF5, CCND1, FLI1, MAFB, BCL2, ETV1, FOXO1, MECOM, CBFB*
Chromosomal rearrangement	0.000	3.727	*SATB2, CCND1, FLI1, BRD3, BCL2, MSI2, ETV1, FOXO1, MECOM, CHCHD7, HMGA1, CBFB*
Cytoplasmic vesicle	0.020	2.912	*SLC2A8, TM9SF1, ICA1, NPTX1, CADPS2, PRDX6, AGTRAP, PHLDA1*
Homeobox	0.022	2.864	*TSHZ3, IRX3, SATB2, MSX1, HOXB7, ZHX2, MKX, ZEB1*
Developmental protein	0.000	2.447	*TSHZ3, FZD8, IRX3, SATB2, EGFL7, ANO1, FOXA1, NTNG1,*

			ANPEP, MECOM, PPDPF, SPRY4, ZIC2, ARHGAP22, NOTCH1, MSX1, HOXB7, SFRP1, POGK, RIPPLY2, MKX, TWIST2
Activator	0.007	2.333	*MAFB, FOXA1, PPARG, KLF15, CPEB1, ZEB1, CITED4, NOTCH1, FLI1, GATA3, DNER, ETV1, NFIL3, ETV4*
Repressor	0.029	2.191	*IRX3, SATB2, MSX1, MAFB, FOXA1, ZHX2, ZNF503, CPEB1, ZEB1, NFIL3, TWIST2*
DNA binding	0.099	2.039	*MSX1, FLI1, HOXB7, PPARG, NR3C2, ZEB1, NR2F2, HMGA1*

SP-PIR, Swiss-Prot Protein Information Resource

Validation by TCGA

Numbers of PTC with *BRAF* mutation in TGGA was 251 and PTC with *BRAF* wild type was 243. In silico validation using TCGA data showed that 491 of 697 genes (70.44%) presented the same promoter hypermethylation with a gene down-regulation pattern in PTC with the $BRAF^{V600E}$ mutated PTC, compared to the PTC tissue without the $BRAF^{V600E}$ mutation. Furthermore, 153 of 227 genes (67.40%) showed hypomethylation with a gene up-regulation pattern in PTC with the $BRAF^{V600E}$ mutated tumors. Details of TCGA validation results for 924 genes described in table 7.

Table 7. Validation of inverse correlation pattern of 924 genes in Nthy/V600E cell and TCGA PTC with *BRAF* mutation tissue.

Hypermethyl-downregulated		**Hypomethyl-upregulated**	
Genes	Logics for inverse correlation pattern, 491/697 (70.44%)	Genes	Logics for inverse correlation pattern, 153/227 (67.40%)
SGCE	TRUE	*SLC6A15*	FALSE
EPB41L3	TRUE	*NTNG1*	TRUE
FASTK	TRUE	*BCL2*	TRUE
DPYSL4	TRUE	*CCND1*	TRUE
PTEN	FALSE	*GAD1*	TRUE
KIAA1217	TRUE	*KCNK1*	TRUE
NTF3	FALSE	*SLAIN1*	FALSE
FAM163A	TRUE	*SPRY4*	TRUE
PAOX	TRUE	*THBD*	TRUE
RUNX3	TRUE	*ANO1*	FALSE
ZFP3	FALSE	*CA2*	TRUE
PRMT6	TRUE	*NACC2*	TRUE
UNC45A	FALSE	*PLXNA2*	TRUE
MEST	TRUE	*SKAP2*	TRUE
CYP24A1	TRUE	*C9orf64*	FALSE
FAM110A	TRUE	*HOXB7*	FALSE
FBLN2	TRUE	*NPAS2*	FALSE
SAMD11	TRUE	*TMEM108*	FALSE
MAD2L2	TRUE	*ADCY1*	FALSE
SCARF2	FALSE	*ALDH1A3*	TRUE
INA	TRUE	*ARHGAP22*	TRUE
FAM84B	TRUE	*CERS2*	FALSE
TP53INP1	FALSE	*CPEB1*	TRUE
GRB10	TRUE	*DUSP6*	TRUE
CENPV	TRUE	*GHR*	TRUE

NDRG2	TRUE	*HAS3*	TRUE
PTH1R	TRUE	*HMGA1*	TRUE
CDO1	TRUE	*ICA1*	TRUE
RPP25	TRUE	*KANK1*	FALSE
IGFBP3	TRUE	*KCTD12*	TRUE
PRKCZ	FALSE	*KHDRBS3*	TRUE
ROR2	TRUE	*MRPS14*	TRUE
LRRC61	FALSE	*NR2F2*	TRUE
RASD2	TRUE	*PSMD5*	TRUE
JDP2	TRUE	*RIPPLY2*	FALSE
FAM133B	TRUE	*SATB2*	FALSE
PAPLN	TRUE	*SLC39A8*	TRUE
CHFR	TRUE	*ANPEP*	TRUE
PPM1E	TRUE	*C3orf52*	TRUE
MGMT	TRUE	*DPYSL3*	TRUE
CLDN11	TRUE	*EPDR1*	FALSE
PLBD1	TRUE	*FERMT1*	TRUE
FAT4	TRUE	*IRX3*	FALSE
AHDC1	TRUE	*LRRC34*	TRUE
LEPR	FALSE	*MKX*	TRUE
CHST13	TRUE	*NAV2*	TRUE
CPT1C	TRUE	*POGK*	TRUE
IRF8	TRUE	*SEC16A*	TRUE
COL1A1	TRUE	*SQRDL*	TRUE
P4HA2	TRUE	*TM9SF1*	FALSE
COL16A1	TRUE	*ABCA1*	TRUE
CTHRC1	TRUE	*ADORA2B*	TRUE
C1QL1	TRUE	*AGTRAP*	TRUE
CCDC85C	FALSE	*AKAP12*	FALSE
PMP22	TRUE	*ARHGDIA*	FALSE
MN1	FALSE	*ARID3A*	TRUE

TRABD	TRUE	*ATRIP*	TRUE
KRBA1	FALSE	*BRD3*	TRUE
FUCA1	TRUE	*C3orf70*	TRUE
C9orf142	TRUE	*C9orf85*	FALSE
GNG7	TRUE	*CADPS2*	TRUE
FZD9	TRUE	*CBFB*	TRUE
HPSE	TRUE	*CORO2B*	TRUE
MGAT1	TRUE	*DUSP1*	TRUE
TSTD1	FALSE	*ETV4*	TRUE
FADS2	TRUE	*FAM102A*	FALSE
MYADM	TRUE	*FAM129A*	TRUE
EXO5	FALSE	*FAM184A*	FALSE
MBP	TRUE	*FAM43B*	TRUE
FAIM	FALSE	*FGF5*	TRUE
EIF4E3	TRUE	*FOXA1*	TRUE
FNDC4	TRUE	*FRMD3*	TRUE
GCHFR	FALSE	*FZD8*	TRUE
MAGOH	TRUE	*GALC*	FALSE
MCOLN3	TRUE	*GLDC*	TRUE
FSTL1	TRUE	*LPAR1*	FALSE
PRSS23	TRUE	*LRRCC1*	FALSE
LOC728392	FALSE	*MANSC1*	TRUE
ANXA3	TRUE	*MLPH*	TRUE
STXBP2	TRUE	*MSI2*	TRUE
BLVRA	FALSE	*MTSS1*	TRUE
GFRA1	TRUE	*PHLDA1*	TRUE
RBCK1	FALSE	*PKIA*	FALSE
RASSF7	FALSE	*PLD6*	TRUE
NGF	TRUE	*PNMAL1*	TRUE
AP1M2	FALSE	*PRKD1*	FALSE
CASZ1	FALSE	*QPCT*	TRUE

ALDH2	TRUE	*RPL31*	FALSE
GPX7	TRUE	*S1PR3*	FALSE
SPINT2	TRUE	*SLC38A1*	TRUE
EFNA1	TRUE	*SOX9*	FALSE
RAP1GAP	TRUE	*ST3GAL1*	TRUE
WNT5A	TRUE	*ST8SIA5*	TRUE
COX17	TRUE	*TOX2*	FALSE
ETS2	FALSE	*TWIST2*	TRUE
TSPAN9	FALSE	*VPS37B*	TRUE
PLEK2	FALSE	*ZEB1*	TRUE
IQCA1	FALSE	*ZHX2*	TRUE
LBH	TRUE	*ABCG1*	FALSE
FARP1	TRUE	*AGPAT9*	TRUE
TFAP2A	FALSE	*AHNAK2*	TRUE
PLAGL1	FALSE	*AK1*	FALSE
NRG1	FALSE	*AK5*	FALSE
APLP1	TRUE	*ALDH3A2*	TRUE
RAB15	TRUE	*ASB13*	TRUE
S100A10	TRUE	*ASTN2*	TRUE
MAP6D1	FALSE	*C19orf24*	TRUE
SGSM3	TRUE	*C9orf89*	FALSE
STOX2	FALSE	*CAMK2N2*	FALSE
ABCG1	FALSE	*CANT1*	TRUE
SLC29A2	TRUE	*CCDC8*	TRUE
CNIH2	FALSE	*CHCHD7*	TRUE
SAP25	FALSE	*CHGB*	TRUE
CHKA	TRUE	*CHSY3*	FALSE
PARP9	TRUE	*CITED4*	TRUE
SOX12	TRUE	*CKB*	TRUE
NINL	FALSE	*CMBL*	TRUE
RHEB	TRUE	*CPXM1*	TRUE

FAM83H	TRUE	*DDN*	TRUE
PLXND1	FALSE	*DECR1*	TRUE
TP53I11	TRUE	*DLAT*	FALSE
GRINA	TRUE	*DNER*	FALSE
GCC1	TRUE	*DYNC1I1*	FALSE
SLC30A3	TRUE	*EGFL7*	FALSE
SCRN1	TRUE	*EGFR*	TRUE
GDF6	FALSE	*EIF5A2*	TRUE
ZNF32	TRUE	*ELMO1*	TRUE
PDLIM1	TRUE	*ERRFI1*	TRUE
UBE2L6	TRUE	*ETV1*	TRUE
DYSF	FALSE	*FAM92A1*	TRUE
UPP1	TRUE	*FBLN5*	FALSE
VANGL2	TRUE	*FBXL16*	TRUE
MT1F	TRUE	*FBXO33*	TRUE
PALM	TRUE	*FGFRL1*	TRUE
ATOH8	TRUE	*FLI1*	TRUE
JUP	TRUE	*FLRT2*	FALSE
MEGF6	TRUE	*FOXO1*	TRUE
TCEA2	TRUE	*FOXQ1*	TRUE
DSP	TRUE	*FTL*	FALSE
ACAT2	FALSE	*GABBR2*	TRUE
IGFBP7	TRUE	*GALNT14*	TRUE
STRA13	TRUE	*GALNT6*	TRUE
PPL	TRUE	*GATA3*	TRUE
ADAMTS5	TRUE	*GLUD1*	TRUE
CDC25B	TRUE	*GPR19*	TRUE
CCDC136	TRUE	*GTF3C6*	FALSE
DLK2	FALSE	*HERC5*	TRUE
ENO2	TRUE	*HJURP*	TRUE
CENPB	FALSE	*HRASLS*	TRUE

PFKP	TRUE	*HSPA4L*	FALSE
CHCHD10	TRUE	*HTRA1*	TRUE
CLDN23	FALSE	*IER2*	TRUE
IL6ST	TRUE	*ITGA2*	TRUE
SLC4A11	TRUE	*KATNB1*	FALSE
C7orf57	FALSE	*KLF15*	TRUE
PBX4	TRUE	*KLHL21*	TRUE
PTPRA	TRUE	*LMBRD2*	FALSE
MFSD10	TRUE	*LYSMD2*	TRUE
OCLN	TRUE	*MAFB*	TRUE
FGFR4	TRUE	*MARCH06*	FALSE
PRR36	FALSE	*MARK1*	TRUE
DIABLO	TRUE	*MDGA2*	FALSE
ANKDD1A	TRUE	*MECOM*	FALSE
PRR5	FALSE	*MIRLET7I*	FALSE
CRLS1	FALSE	*MRAP2*	FALSE
RAB6B	TRUE	*MSX1*	TRUE
SMARCD3	TRUE	*MYRIP*	TRUE
PPP1R3C	TRUE	*NALCN*	TRUE
FDFT1	TRUE	*NEDD4L*	TRUE
YBX2	TRUE	*NFIL3*	TRUE
BCAT1	TRUE	*NOTCH1*	TRUE
EHBP1L1	TRUE	*NPTX1*	TRUE
SUN1	FALSE	*NPY*	TRUE
SPIRE1	TRUE	*NR3C2*	TRUE
GREB1L	TRUE	*NTSR1*	TRUE
TES	TRUE	*OPCML*	FALSE
SCARA3	TRUE	*OSR1*	TRUE
FAM64A	TRUE	*PACSIN3*	TRUE
SLC22A17	TRUE	*PAIP1*	TRUE
KLC3	TRUE	*PDE12*	FALSE

CYP51A1	TRUE	*PLXNA4*	FALSE
CCNF	FALSE	*PPARG*	TRUE
PTPRN	TRUE	*PPDPF*	FALSE
CD40	TRUE	*PPFIBP2*	FALSE
ELOVL2	TRUE	*PPM1A*	TRUE
SNTA1	TRUE	*PPP2R2B*	TRUE
IFI30	TRUE	*PRDX6*	TRUE
KCNH3	TRUE	*PRR16*	FALSE
FTH1	TRUE	*RAI14*	TRUE
EBF4	FALSE	*RAPGEF5*	FALSE
JMJD8	FALSE	*RAVER1*	FALSE
MYBL2	TRUE	*RGS17*	TRUE
ASS1	TRUE	*RTN1*	FALSE
ACOT4	FALSE	*SAMD10*	FALSE
ATF3	FALSE	*SFRP1*	TRUE
HSD11B1L	TRUE	*SH3BGRL2*	TRUE
MYO1C	TRUE	*SLC16A9*	TRUE
UQCRC1	TRUE	*SLC2A8*	TRUE
ADCK2	TRUE	*SLC35A3*	TRUE
MEG3	TRUE	*SLC35F3*	FALSE
CABP7	FALSE	*SLC7A2*	TRUE
MRAS	FALSE	*SNHG7*	FALSE
FGF18	TRUE	*SNTB1*	FALSE
DGAT1	TRUE	*SOCS4*	TRUE
SLC38A3	TRUE	*STOM*	TRUE
LRRN2	TRUE	*TENM4*	FALSE
FAM50B	TRUE	*TMEM115*	TRUE
NPPB	TRUE	*TMEM163*	TRUE
CYP1B1	TRUE	*TMEM2*	TRUE
CRISPLD2	FALSE	*TMEM238*	FALSE
CXXC5	TRUE	*TNFRSF11B*	TRUE

BNIP3	FALSE	*TRIM7*	FALSE
AFAP1L2	TRUE	*TSEN2*	TRUE
KRT7	TRUE	*TSHZ3*	FALSE
AIF1L	FALSE	*UBE2E3*	FALSE
BIN1	TRUE	*WNK4*	TRUE
TUBA4A	TRUE	*WSCD1*	FALSE
FBLN1	TRUE	*XPOT*	FALSE
NUAK1	TRUE	*ZDBF2*	TRUE
F2R	FALSE	*ZFP36L1*	TRUE
STC2	TRUE	*ZIC2*	FALSE
SMAD6	TRUE	*ZMYND19*	FALSE
CAND2	TRUE	*ZNF503*	TRUE
RNF144B	FALSE	*ZNF544*	TRUE
HOXC8	FALSE	*ZNF583*	TRUE
SLC37A3	FALSE	*ZNF704*	FALSE
CD14	FALSE	*ZSCAN18*	TRUE
SMO	TRUE		
CUX1	TRUE		
INHBB	FALSE		
GLIS3	FALSE		
SLC12A8	FALSE		
ADD3	FALSE		
VGLL2	FALSE		
EPHB4	TRUE		
ZBTB46	FALSE		
TWSG1	FALSE		
HOMER2	TRUE		
HES4	TRUE		
SCPEP1	TRUE		
SRI	TRUE		
SH3BP4	TRUE		

SSBP2	TRUE		
SIDT2	FALSE		
ZNF467	TRUE		
MAP1B	FALSE		
MAP1LC3A	TRUE		
PITPNM1	TRUE		
KLHDC8B	TRUE		
COL6A1	TRUE		
ME1	TRUE		
NRSN2	FALSE		
C1QL4	TRUE		
ARHGEF16	TRUE		
ZNF395	TRUE		
PCYOX1L	TRUE		
VEGFB	TRUE		
TPM2	TRUE		
EFHD1	FALSE		
GPX3	TRUE		
NMU	TRUE		
C11orf68	TRUE		
MARCKSL1	TRUE		
CHAF1B	TRUE		
ARHGEF10	FALSE		
RGS7	TRUE		
IDH2	TRUE		
HSPA2	TRUE		
DDX41	TRUE		
PER3	FALSE		
ATP6V1A	TRUE		
ZBTB42	TRUE		
PAPSS2	TRUE		

NDUFA12	TRUE		
ZFP90	TRUE		
KAZN	FALSE		
ALDOA	TRUE		
P2RX6	FALSE		
LITAF	TRUE		
C17orf100	FALSE		
MOXD1	TRUE		
ECHDC3	TRUE		
FHOD1	TRUE		
SULF2	TRUE		
ADCY9	TRUE		
SNRPB2	FALSE		
ITGB4	TRUE		
POFUT2	TRUE		
ZC3H12A	TRUE		
RHPN2	FALSE		
PRUNE2	TRUE		
RALBP1	TRUE		
SBK1	TRUE		
DTD1	TRUE		
NSUN5	FALSE		
ARNT2	TRUE		
GDPD5	TRUE		
STK25	TRUE		
STMND1	FALSE		
TUB	TRUE		
ZBTB48	TRUE		
AGAP3	TRUE		
SERPINB6	TRUE		
LAYN	TRUE		

TTC39C	TRUE		
URGCP	TRUE		
AZIN2	FALSE		
DDAH2	TRUE		
RNF207	FALSE		
TNFRSF19	TRUE		
ADAMTS2	TRUE		
FAM175B	FALSE		
TAX1BP1	TRUE		
CLEC16A	TRUE		
LPAR2	TRUE		
HEYL	FALSE		
RFC4	FALSE		
EBF1	TRUE		
LRRC32	TRUE		
ATRN	TRUE		
WDR33	TRUE		
SLC16A3	TRUE		
CYB5R3	FALSE		
SMAD7	TRUE		
GPRIN2	TRUE		
KANK2	TRUE		
RND2	TRUE		
XRN2	TRUE		
TMSB10	TRUE		
STARD10	TRUE		
GSTM3	FALSE		
ERI3	TRUE		
A4GALT	FALSE		
VPS28	TRUE		
LZTS2	TRUE		

DSC2	TRUE		
KATNAL1	TRUE		
SLC25A40	TRUE		
VASH1	FALSE		
ATP5A1	TRUE		
ISYNA1	TRUE		
KRIT1	TRUE		
SLC6A9	TRUE		
FADS3	TRUE		
PTPN2	TRUE		
DDHD2	FALSE		
LPPR5	TRUE		
ATG5	FALSE		
NADK	FALSE		
PPP3CC	TRUE		
FRMD8	TRUE		
RELL2	TRUE		
MRPS6	TRUE		
ADAMTS7	TRUE		
TUBB2B	FALSE		
CD70	TRUE		
ACKR3	FALSE		
MATN2	TRUE		
PLAC8	TRUE		
CGNL1	TRUE		
PALLD	TRUE		
MAL	FALSE		
PTPRE	TRUE		
VASN	TRUE		
PYCARD	TRUE		
MLLT11	FALSE		

FSTL3	TRUE		
H1F0	TRUE		
ISL1	TRUE		
ABCC3	TRUE		
ADA	TRUE		
SCD	TRUE		
PTPRM	FALSE		
CELSR2	TRUE		
FOXN3	TRUE		
CDH2	TRUE		
CXCL16	TRUE		
RAB31	TRUE		
ZNF789	TRUE		
MYL9	FALSE		
PEG10	TRUE		
TUBB2A	FALSE		
RAB11FIP1	TRUE		
MALL	FALSE		
PRRX2	TRUE		
ZNF362	TRUE		
DOCK2	TRUE		
SLC7A5	TRUE		
DSTN	TRUE		
FGFR3	TRUE		
HLA-B	TRUE		
ABHD12	TRUE		
PGM1	FALSE		
CDC42EP5	FALSE		
RBPMS2	TRUE		
PGAM1	FALSE		
PRDX5	TRUE		

SLC22A5	FALSE		
EFNB3	FALSE		
LDOC1L	TRUE		
PLXNB2	TRUE		
MX1	TRUE		
HSPB1	TRUE		
SLC25A13	TRUE		
OLFML2B	TRUE		
PHLDB1	FALSE		
CARD10	TRUE		
GPRC5C	FALSE		
TMEM45A	TRUE		
BMPER	FALSE		
COL9A2	FALSE		
HMGCR	TRUE		
SERPINH1	FALSE		
WWC1	FALSE		
CHST15	TRUE		
RBP7	TRUE		
GYPC	TRUE		
FAM46B	TRUE		
MIF	TRUE		
XPNPEP1	FALSE		
EFEMP2	FALSE		
NIPAL3	TRUE		
SMIM1	FALSE		
NPTN	TRUE		
TMEM91	TRUE		
PLCE1	TRUE		
CDK5RAP3	TRUE		
RARRES2	TRUE		

RHOD	TRUE		
TUBB6	TRUE		
GUSB	FALSE		
IDH1	TRUE		
CDK14	TRUE		
MXD3	TRUE		
PLA2G16	FALSE		
ETNK2	TRUE		
MCM7	TRUE		
OLFML2A	TRUE		
SCMH1	FALSE		
MKRN1	TRUE		
C17orf97	TRUE		
PRICKLE1	TRUE		
PLEKHA1	TRUE		
ERBB2	TRUE		
SMAD3	TRUE		
ADD1	TRUE		
CHN1	FALSE		
PPP1R12B	TRUE		
PTGIS	FALSE		
RARA	TRUE		
SELM	TRUE		
PKD2	TRUE		
HBP1	TRUE		
CCDC74B	FALSE		
USP46	TRUE		
ZNF775	TRUE		
CAMTA1	FALSE		
SLC26A11	TRUE		
INSIG1	TRUE		

CPE	TRUE		
UBE4B	TRUE		
ZNF133	TRUE		
RBX1	FALSE		
UQCRQ	FALSE		
CYTL1	FALSE		
PANX2	FALSE		
NT5DC2	FALSE		
LYSMD4	FALSE		
HIP1R	TRUE		
SREBF1	TRUE		
RILPL1	TRUE		
ABHD8	TRUE		
LRRC42	FALSE		
C14orf132	FALSE		
MDK	TRUE		
ZC3HC1	TRUE		
PGRMC2	TRUE		
CD276	FALSE		
UBE2H	TRUE		
INTS12	FALSE		
HLA-H	TRUE		
NFIB	TRUE		
SSPN	TRUE		
CADM1	TRUE		
TMEM120A	TRUE		
CAV1	TRUE		
MTMR3	TRUE		
PDGFB	TRUE		
OCEL1	TRUE		
RIMKLA	TRUE		

SPNS1	TRUE		
UBE2F	TRUE		
CTNNA1	TRUE		
DGCR2	TRUE		
GDF15	TRUE		
NCOA4	TRUE		
TBCA	FALSE		
MCM8	TRUE		
OPRL1	FALSE		
TM7SF2	TRUE		
ITFG3	TRUE		
GNB2	FALSE		
AHNAK	TRUE		
TESK1	FALSE		
KDM5B	TRUE		
AFF4	TRUE		
TDG	FALSE		
DVL2	TRUE		
MOCOS	FALSE		
CGN	TRUE		
H2AFY2	FALSE		
FAM53B	TRUE		
RYBP	TRUE		
SHANK3	TRUE		
DBI	TRUE		
GGA2	FALSE		
LIMS2	TRUE		
CLK3	TRUE		
ASPHD2	TRUE		
SPIDR	FALSE		
C4orf48	FALSE		

VGF	TRUE		
ADAMTSL4	FALSE		
NCAPG2	TRUE		
FBXO6	TRUE		
POLR2J	TRUE		
PON2	TRUE		
ARID1A	FALSE		
CKAP4	FALSE		
TECPR1	FALSE		
PHF13	TRUE		
RNF130	FALSE		
BBS9	TRUE		
DUSP18	TRUE		
HSPB11	TRUE		
COMMD4	FALSE		
RERE	FALSE		
RUFY1	TRUE		
BRI3	FALSE		
RASSF4	TRUE		
SLC27A3	TRUE		
CECR5	TRUE		
ATOX1	TRUE		
DAGLA	TRUE		
MTUS1	TRUE		
SAMM50	TRUE		
GALNT11	TRUE		
C7orf50	TRUE		
MUM1	TRUE		
B4GALT7	FALSE		
EPB41L5	FALSE		
AP2M1	TRUE		

ZFYVE16	FALSE		
MAPK6	FALSE		
PRRT3	TRUE		
PDXP	TRUE		
KREMEN2	TRUE		
PIK3CD	TRUE		
GAA	TRUE		
DBNDD1	TRUE		
NANP	TRUE		
FKBP14	FALSE		
GPS2	FALSE		
PLEKHA2	FALSE		
TMEM134	FALSE		
KIAA1147	TRUE		
NQO2	TRUE		
TPM1	FALSE		
PFN1	FALSE		
WTIP	TRUE		
AP4E1	TRUE		
ERBB3	TRUE		
MIER1	TRUE		
TMEM8B	TRUE		
ACTB	FALSE		
VASH2	TRUE		
JOSD1	TRUE		
TMEM97	FALSE		
LRRC20	FALSE		
FLYWCH2	TRUE		
SNX7	TRUE		
CABLES2	FALSE		
ARL4A	TRUE		

SUSD3	TRUE		
HDHD2	TRUE		
SERAC1	TRUE		
GTF2IRD1	TRUE		
MYL12A	TRUE		
TEAD3	TRUE		
TFIP11	FALSE		
EML4	TRUE		
PDCD4-AS1	FALSE		
MTG1	TRUE		
PXYLP1	FALSE		
GLOD4	TRUE		
DYM	FALSE		
CPT1B	FALSE		
ABCC5	FALSE		
MPST	FALSE		
RAP1GDS1	TRUE		
OBSL1	TRUE		
HMGN2	FALSE		
CAST	TRUE		
MKL2	FALSE		
LOC284023	TRUE		
IER3	TRUE		
PSMA5	FALSE		
ALG10B	TRUE		
DDR1	TRUE		
RRAGC	TRUE		
B4GALT1	TRUE		
DBF4	TRUE		
TET1	FALSE		
FBXO2	TRUE		

CCM2	TRUE		
GCSH	TRUE		
TEF	FALSE		
SELO	TRUE		
ITGB3	TRUE		
ZNF280B	FALSE		
RRBP1	FALSE		
IL15	FALSE		
BACE2	TRUE		
FAM178A	TRUE		
RAB20	TRUE		
FLNB	TRUE		
LSM5	TRUE		
SYT11	TRUE		
PEX6	FALSE		
MMP2	TRUE		
SLFN13	FALSE		
UBXN2A	FALSE		
AGFG2	FALSE		
RSPH3	TRUE		
CORO1A	TRUE		
MTF2	FALSE		
CTSH	TRUE		
TMEM107	FALSE		
RCOR2	FALSE		
C18orf25	FALSE		
ATXN10	FALSE		
LYPD1	TRUE		
DNMT3B	TRUE		
CSTB	TRUE		
NICN1	TRUE		

TIMM8B	TRUE		
MSRB1	FALSE		
MTSS1L	TRUE		
DNAJB6	TRUE		
PLIN2	TRUE		
WDR91	TRUE		
HAPLN3	TRUE		
H2AFY	TRUE		
RADIL	TRUE		
NARF	FALSE		
MT1X	TRUE		
HSF2	FALSE		
MAPRE2	TRUE		
TP53BP1	FALSE		
RPS23	FALSE		
GLI3	TRUE		
PDPR	FALSE		
MIS12	TRUE		
SLCO3A1	FALSE		
PCGF6	TRUE		
CASP2	TRUE		
PPCS	TRUE		
BOK	TRUE		
ZNF580	TRUE		
HOOK1	TRUE		
TMEM222	TRUE		
DNAJC4	TRUE		
ZNF514	FALSE		
LIMK2	TRUE		
LMO1	TRUE		
TMEM256	FALSE		

IFFO2	TRUE		
C1orf159	TRUE		
TTC26	FALSE		
BRE	TRUE		
PLA2G15	FALSE		
PNPLA8	FALSE		
TMEM14A	TRUE		
P2RY6	TRUE		
ZMYM5	TRUE		
TIGD7	TRUE		
SNX5	TRUE		
ALDH4A1	TRUE		
CCDC138	FALSE		
ESCO1	TRUE		
TMCO3	FALSE		
HDAC7	FALSE		
LCMT2	FALSE		
GNAI1	TRUE		
RAN	TRUE		
ZNF514	FALSE		
ZNF775	TRUE		

Validation by Pyrosequencing and RT-PCR

Figure 4 shows the *in-vitro* validation results for part of inversely correlated genes (*RUNX3, MEST, TP53INP1, RASSF4*, and *GPX3* among the hypermethylated genes with downregulation in Nthy/V600E cells; *CCND1, BCL2, DUSP6, EGFR*, and *ZEB1* among the hypomethylated genes with upregulation in Nthy/V600E cells). Pyrosequencing was used for the methylation analysis, and qRT-PCR was used for mRNA expression analysis. *RUNX3, MEST, TP53INP1, RASSF4*, and *GPX3* showed higher promoter methylation rates in Nthy/V600E cells than in control cells (Figure 4A). *RUNX3, MEST, RASSF4*, and *GPX3* also showed lower mRNA expression in Nthy/V600E cells (Figure 4B). *CCND1, BCL2, DUSP6, EGFR*, and *ZEB1* showed lower promoter methylation rates in Nthy/V600E cells, and these genes showed higher mRNA expression in Nthy/V600E cells (Figure 4C and 4D).

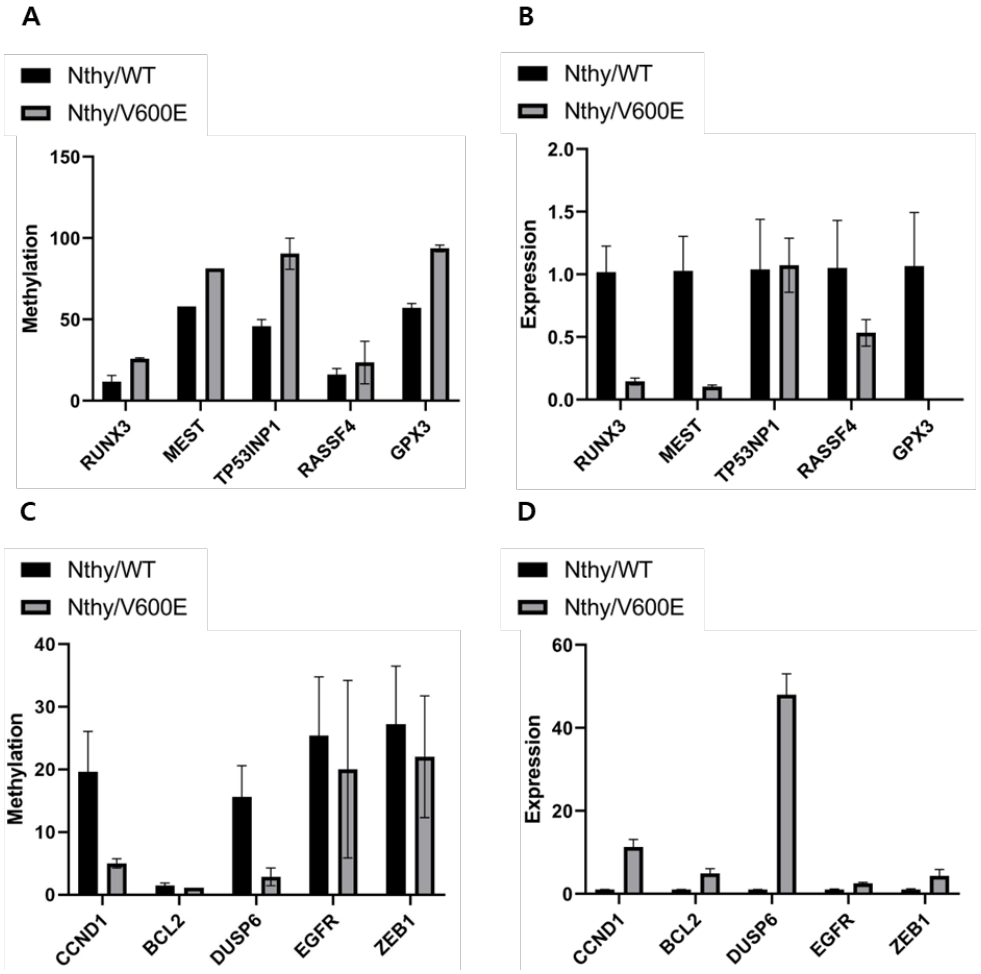

Figure 4. Pyrosequencing and quantitative real-time polymerase chain reaction results for selected genes. (A) Methylation status of selected genes that showed hypermethylation and downregulation in Nthy/V600E cells. (B) mRNA expression status of selected genes that showed hypermethylation and downregulation in Nthy/V600E cells. (C) Methylation status of selected genes that showed

hypomethylation and upregulation in Nthy/V600E cells. (D) mRNA expression status of selected genes that showed hypomethylation and upregulation in Nthy/V600E cells.

Discussion

Somatic *BRAF*^{V600E} mutation is major driver mutation in thyroid cancer in differentiated PTC. Prevalence of *BRAF*^{V600E} mutation in thyroid cancer reported up to 30–80% and known to be associated with aggressive characteristics of thyroid cancer including extrathyroidal extension, advanced stage, lymph node or distant metastasis [3,24–26]. Basic molecular mechanism of *BRAF*^{V600E} mutation in thyroid cancer is activate mitogen–activated protein kinase (MAP kinase)/extracellular–signal–regulated kinase (ERK) pathway. Activation of MAP kinase related gene expression in cell considered as major tumorigenic mechanism of various cancers, with enhanced cell cycle with uncontrolled division and over–proliferation [27,28].

Concurrent genomic and epigenomic change that initiated by *BRAF*^{V600E} mutation in thyroid cancer had been specifically demonstrated in previous research. Gene expression and DNA methylation changes in MAP kinase pathway genes are associate with the specific clinicopathologic characteristics in thyroid cancer [12,29].

TCGA project and other next generation sequencing studies also revealed that specific sets of gene expression alteration patterns are present in thyroid cancer, follows by *BRAF*^{V600E} mutation [6,30]. According to TCGA, *BRAF*^{V600E} like thyroid cancer is related with upregulated ERK related genes including DUSP genes which is initiate the Erk transcription, whereas low thyroid differentiation score. And methylation signature also differentially classified between *BRAF* type and *RAS* type thyroid cancer6. However, intracellular mechanism that how the *BRAF*^{V600E} driver mutation alter the various gene expressions in thyroid cells has not yet been clearly elucidated. TCGA shown that two DNA methylation clusters were gathered in the *BRAF*^{V600E} like thyroid cancer but molecular consequence of CpG methylation and gene expression change was not assessed [6].

DNA methylation is an epigenomic phenomenon that methyl group is attached to the 5th carbon of cytosine residue in CpG dinucleotide. Clusters of CpG dinucleotides are called as "CpG island" and generally located in promotor area. Hypermethylation of promotor CpG island repress the transcription of downstream exon and result in suppress gene expression [8,31]. Hou *et al.* initially proposed that

BRAF^{V600E} mutation may alter the MAP kinase gene expression through DNA methylation [16]. They reported functional association of *BRAF*^{V600E} mutation with methylation change in thyroid cancer cells and suggested that *BRAF*^{V600E} mutation has possible ability to epigenetic change. They used BCPAP and OCUT1 cell lines which harbor the *BRAF*^{V600E} mutation [16]. For the control group, they used shRNA method to knock-down the BRAF gene from the thyroid cancer cell lines. There were studies to demonstrate the correlation between DNA methylation and gene expression in thyroid cancer according to *BRAF*^{V600E} mutation, using patient derived papillary thyroid cancer and normal thyroid tissue as control [12,14,32-34]. These studies found that hyper-methylation of tumor suppressor genes (*PTEN, RASSF1A, TIMP3, SLC5A8, DAPK, RARβ2*, etc.) and hypo-methylation of tumorigenic genes (*VEGF*, etc.) were identified in thyroid cancer with *BRAF*^{V600E} mutation. However, previous studies used the final product of thyroid cancer tissue, that cannot determine the order of genomic consequence of primitive *BRAF*^{V600E} mutation, subsequent methylation, and gene expression alteration is followed. Although Hou *et al*. used the *BRAF* knock-down PTC cell lines, it still

not the initial period of carcinogenesis induced by *BRAF*^{V600E} mutation. As so, previous studies have limitation to explain the cellular consequence, between epigenomic and genomic correlation by the *BRAF*^{V600E} mutation.

To overcome the mentioned limitation above, I used *BRAF* gene transfected Nthy-ori cell-lines (Nthy/WT and Nthy/V600E)19. In our initial research, Nthy/WT cell showed similar biologic behavior with Nthy/Ori cells. In contrast, Nthy/V600E cells showed increased anchorage independent growth, invasion ability and up-regulated genes with ERK/MAPK cascade over time, and gradually becoming a thyroid cancer cell. It can suggest that Nthy Nthy/V600E cell is a good model to study early period biologic consequence, induced by *BRAF*^{V600E} mutation in thyroid cell. Other thyroid cell lines have already been changed into late stage or aggressive type of thyroid cancer such as anaplastic or follicular cancer subtype [18,19].

Our research showed that induction of *BRAF*^{V600E} mutation in Nthy-ori cell result in frequent DNA hypermethylation; 199,821 probes were hypermethylated in Nthy/V600E, compared with 66,446 probes in Nthy/WT. In the correlation analysis between methylation

and gene expression, 697 genes were hypermethylated with under-expressed in Nthy/V600E cells. These genes are related with strong inducer of apoptosis and promote immune mediated response (*FASTK*) [35], tumor suppressor genes in many cancers (*PTEN*) [36], significantly increased CpG methylation state in gastric cancer (*SGCE*) [37], its' inhibition resulted in rapid cell death of progenitor cells (*PAOX*) [38], loss of expression with methylation was related with carcinogenesis (*MEST*) [39,40], and site-specific hypermethylation predicts PTC recurrence (*RUNX3*) [41]. In the protein information analysis, tumor suppressor genes that repress the carcinogenesis (*RASSF4, PRR5, PLA2G16, CADM1, EFNA1, PYCARD, BIN1, MN1, PTEN, MTUS1*) also downregulated in Nthy/V600E cell. On the contrary, 227 genes showed hypomethylated with over-expressed in Nthy/V600E cell. These genes include transport of glucose and other sugars and hypermethylated in cancer (*SLC6A15*) [42], blocks the apoptotic death and differentially methylated in breast cancer (*BCL2*) [43], alters cell cycle progression with contribute to tumorigenesis and hypomethylated-high gene expression (*CCND1*) [44]. Proto-oncogenes that promote

carcinogenesis (*GFR, FGF5, CCND1, FLI1, MAFB, BCL2, ETV1, FOXO1, MECOM, CBFB*) were significantly enriched in protein information analysis.

Selected 10 genes for validation analysis are as follows: *RUNX3, MEST, TP53INP1, RASSF4, GPX3, CCND1, BCL2, DUSP6, EGFR* and *ZEB1*. *RUNX* is one of the tumor suppressor genes that its methylation in thyroid cancer and can predict the recurrence of PTC [41,45,46]. DNA methylation subsequent *MEST* gene expression knockdown is proposed as thyroid cancer cell survival [47]. For the *TP53IP1*, loss of p53 function is important for immortalization in thyroid cancer cell lines [48]. Methylation of Ras association domain family (*RASSF*) genes were reported in thyroid cancer [49]. *GPX3* is frequently methylated in human PTC tissue and expression was regulated by promotor methylation and it was associated with tumor size and lymph node metastasis [50]. *CCND1* gene enhanced expression proposed as a prognostic factor and possible mechanism for recurrent in PTC [51]. Higher expression of *BCL2* gene was associated with poor survival in thyroid cancer and modulated by miRNA regulation mechanism [52]. Increased expression of *DUSP6*

gene with decreased DNA methylation was reported in PTC tissue [32]. Overexpression of *EGFR* in thyroid cancer is well known and associated with tumor aggressiveness and progression [53,54]. Overexpression of *ZEB1* was associated with aggressive tumor progression of PTC and its expression can be knock down by siRNAs or miRNAs [55-57]. For those genes, same methylation alteration patterns were obtained in promotor sites by pyrosequencing, and inverse correlations of mRNA expression were also identified as shown in figure 4. Therefore, we can propose that inverse correlated genes from our microarrays can be reliable finding, with the validation of important genes by pyrosequencing and RT-PCR

I checked the methylation and gene expression changes of significant genes in the TGCA data, part of *in-silico* validation. Results identified that 491 of 697 genes (70.44%) showed the same hypermethylation-downregulation pattern, and 153 of 227 genes (67.40%) showed hypomethylation-upregulation in $BRAF^{V600E}$ mutated PTC tissue. The remaining 30% of genes did not show significant methylation-gene expression changes. This difference is probably because one experiment was performed on cell lines and

another experiment was performed on surgically removed cancer tissue. Although the cancer cell line has very similar properties to those of the cancer tissue from which it originated, it is inevitably genetically different from cancer tissue growing in the human body as a result of being grown in an in vitro environment. Therefore, three-dimensional cell line models such as organoids are being used in recent studies. This finding suggest that future research should investigate these issues using three-dimensional cell lines.

Based on our analysis, it suggest that initiation of the *BRAF*^{V600E} mutation in thyroid cells can modulate cancer-related gene expression by altering promoter site CpG island methylation. The possible carcinogenic mechanism is illustrated in Figure 5.

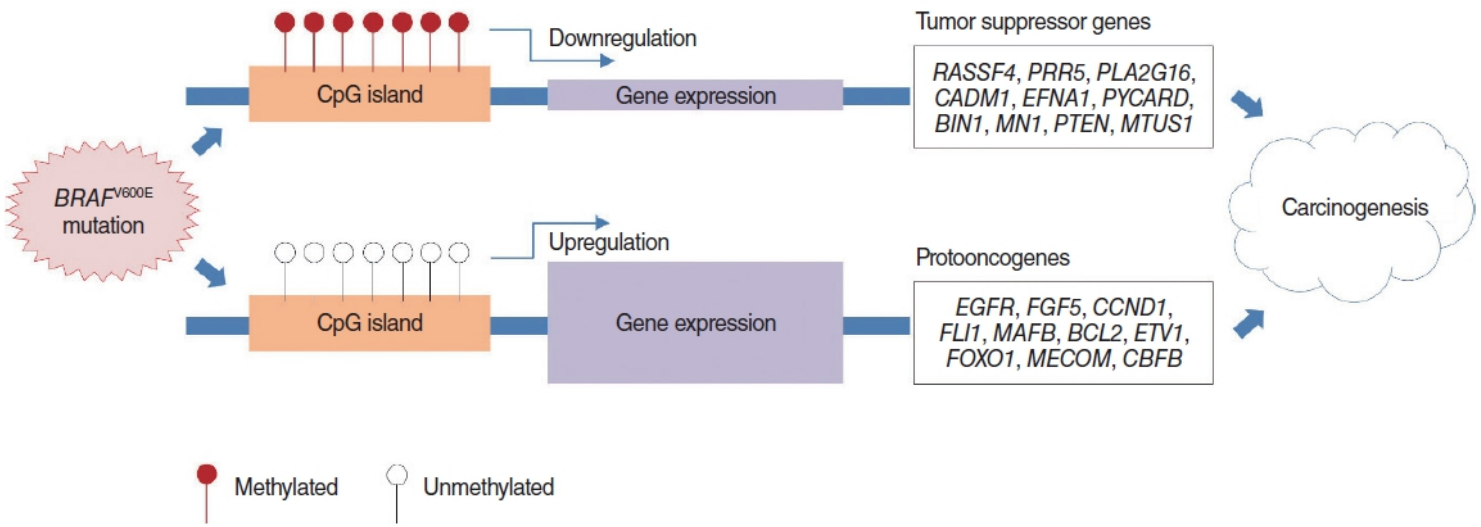

Figure 5. Possible carcinogenic mechanisms of the *BRAF*^{V600E} mutation

There have been many reports of methylation changes caused by *BRAF* mutations in various cancers. However, there has been relatively little research on the mechanism that how the *BRAF* mutation directly or indirectly effects on the DNA methylation change. From the previous literature, *DNMT1* gene act for the maintenance of methylation, and *DNMT3a* and *DNMT3b* are effect on the de-novo methylation. *TET* family genes (*TET1*, *TET2* and *TET3*) have a role of DNA de-methylation. *TET3* act prior to the differentiation and *TET1* act after the differentiation [16]. It also reported that *BRAF* mutation results in the deregulation of the *TET* genes (*TET1*, *TET2*, and *TET3*), which encode DNA demethylases, leading to demethylation in colon cancer [58]. Another report implies that the *BRAF* oncoprotein activates the transcriptional repressor *MAFG* to mediate CpG island methylation and make a epigenetic silencing [59]. Association study of DNA methylation pathway related genes and *BRAF* mutation should be required to identify the biological connections between *BRAF* mutation and DNA methylation. Moreover, further study with histone modifications and microRNAs with *BRAF* mutation also be helpful to find the mechanism of epigenomic

modulation by the *BRAF* mutation.

According to our analysis, it suggests that initiation of $BRAF^{V600E}$ mutation in thyroid cell can modulate cancer related gene expressions by changing promotor site CpG island methylation. $BRAF^{V600E}$ mutation suppress the anti-tumor related gene expression by promotor hypermethylation whereas enhance the tumorigenic effect genes by hypomethylation. In particularly, this study strongly supports this argument unlike the previous research, as this study experimented with both gene expression and methylation arrays in the process of cancer-processing normal thyroid cells, induced by $BRAF^{V600E}$ driver mutation which is the highest trigger in MAPK pathway. This study also the first report that uses the latest methylation array chip – Infinium MethylationEPIC BeadChip (850k) in thyroid cancer study. Using the higher density chip, this study also able to more detailed analysis of promotor site methylation, compared with previous studies that used the 27K or 450K chips [12,33,34].

The results of our study are suggested to have the following clinical implications. If a test method using a DNA methylation biomarker related to the *BRAF* mutation is developed and applied in

the clinical field, the diagnostic accuracy for ambiguous thyroid nodules could be improved. Thus, unnecessary re-testing or diagnostic surgery could be reduced. In addition, the *BRAF* mutation is expected to be used as a biomarker to determine the prognosis and future treatment policies for patients undergoing surgery for thyroid cancer. Finally, since methylation changes are epigenetic, meaning that they are easier to modify than DNA mutations or gene expression alterations, there may be the potential to develop a methylation-targeted therapeutic agent to control CpG islands located on carcinogenic genes.

This study has certain limitations. Although our cell lines are good models for studying the genomic consequences of the $BRAF^{V600E}$ mutation, they are not yet standardized worldwide. Further studies including previously known *BRAF* mutation-dominant, or *RAS* mutation-dominant thyroid cancer cell lines are needed to support our results [18]. In addition, our study could not conclude that methylation changes due to *BRAF* gene mutations can be reversed by *BRAF* gene suppression (e.g., with *BRAF* inhibitor treatment). Finally, this study did not identify the direct mechanisms of how the *BRAF*

mutation affects methylation in thyroid cancer cell lines, because our study dealt with associations using two types of microarrays. I intend to address these limitations in our subsequent research.

In summary, induction of the *BRAF*^{V600E} mutation in normal thyroid cells changed gene expression by affecting the frequency of DNA methylation of promoter site CpG islands. This result suggests that the *BRAF*^{V600E} mutation modulates DNA methylation to change gene expression in the carcinogenic cascade. In future research, this result will be used to identify potential diagnostic and therapeutic targets in thyroid cancer.

References

1. Kitahara CM, Sosa JA: The changing incidence of thyroid cancer. Nat Rev Endocrinol 12:646-653, 2016

2. Jung KW, Won YJ, Kong HJ, et al: Cancer Statistics in Korea: Incidence, Mortality, Survival, and Prevalence in 2015. Cancer Res Treat 50:303-316, 2018

3. Xing M: BRAF mutation in thyroid cancer. Endocr Relat Cancer 12:245-62, 2005

4. Li C, Lee KC, Schneider EB, et al: BRAF V600E mutation and its association with clinicopathological features of papillary thyroid cancer: a meta-analysis. J Clin Endocrinol Metab 97:4559-70, 2012

5. Jung CK, Little MP, Lubin JH, et al: The increase in thyroid cancer incidence during the last four decades is accompanied by a high frequency of BRAF mutations and a sharp increase in RAS mutations. J Clin Endocrinol Metab 99:E276-85, 2014

6. Cancer Genome Atlas Research N: Integrated genomic characterization of papillary thyroid carcinoma. Cell 159:676-90,

2014

7. Faam B, Ghaffari MA, Ghadiri A, et al: Epigenetic modifications in human thyroid cancer. Biomed Rep 3:3-8, 2015

8. Bird A: DNA methylation patterns and epigenetic memory. Genes Dev 16:6-21, 2002

9. Xing M: Gene methylation in thyroid tumorigenesis. Endocrinology 148:948-53, 2007

10. Chen YC, Gotea V, Margolin G, et al: Significant associations between driver gene mutations and DNA methylation alterations across many cancer types. PLoS Comput Biol 13:e1005840, 2017

11. Chai L, Li J, Lv Z: An integrated analysis of cancer genes in thyroid cancer. Oncol Rep 35:962-70, 2016

12. Ellis RJ, Wang Y, Stevenson HS, et al: Genome-wide methylation patterns in papillary thyroid cancer are distinct based on histological subtype and tumor genotype. J Clin Endocrinol Metab 99:E329-37, 2014

13. Beltrami CM, Dos Reis MB, Barros-Filho MC, et al: Integrated

data analysis reveals potential drivers and pathways disrupted by DNA methylation in papillary thyroid carcinomas. Clin Epigenetics 9:45, 2017

14. Kikuchi Y, Tsuji E, Yagi K, et al: Aberrantly methylated genes in human papillary thyroid cancer and their association with BRAF/RAS mutation. Front Genet 4:271, 2013

15. White MG, Nagar S, Aschebrook-Kilfoy B, et al: Epigenetic Alterations and Canonical Pathway Disruption in Papillary Thyroid Cancer: A Genome-wide Methylation Analysis. Ann Surg Oncol 23:2302-9, 2016

16. Hou P, Liu D, Xing M: Genome-wide alterations in gene methylation by the BRAF V600E mutation in papillary thyroid cancer cells. Endocr Relat Cancer 18:687-97, 2011

17. Ozer B, Sezerman OU: A novel analysis strategy for integrating methylation and expression data reveals core pathways for thyroid cancer aetiology. BMC Genomics 16 Suppl 12:S7, 2015

18. Saiselet M, Floor S, Tarabichi M, et al: Thyroid cancer cell lines: an overview. Front Endocrinol (Lausanne) 3:133, 2012

19. Kim BA, Jee HG, Yi JW, et al: Expression Profiling of a Human Thyroid Cell Line Stably Expressing the BRAFV600E Mutation. Cancer Genomics Proteomics 14:53-67, 2017

20. Ritchie ME, Phipson B, Wu D, et al: limma powers differential expression analyses for RNA-sequencing and microarray studies. Nucleic Acids Res 43:e47, 2015

21. Morris TJ, Butcher LM, Feber A, et al: ChAMP: 450k Chip Analysis Methylation Pipeline. Bioinformatics 30:428-30, 2014

22. Huang da W, Sherman BT, Lempicki RA: Systematic and integrative analysis of large gene lists using DAVID bioinformatics resources. Nat Protoc 4:44-57, 2009

23. Yip YL, Scheib H, Diemand AV, et al: The Swiss-Prot variant page and the ModSNP database: a resource for sequence and structure information on human protein variants. Hum Mutat 23:464-70, 2004

24. Nikiforova MN, Kimura ET, Gandhi M, et al: BRAF mutations in thyroid tumors are restricted to papillary carcinomas and anaplastic or poorly differentiated carcinomas arising from papillary carcinomas.

J Clin Endocrinol Metab 88:5399-404, 2003

25. Kim KH, Kang DW, Kim SH, et al: Mutations of the BRAF gene in papillary thyroid carcinoma in a Korean population. Yonsei Med J 45:818-21, 2004

26. Namba H, Nakashima M, Hayashi T, et al: Clinical implication of hot spot BRAF mutation, V599E, in papillary thyroid cancers. J Clin Endocrinol Metab 88:4393-7, 2003

27. Hilger RA, Scheulen ME, Strumberg D: The Ras-Raf-MEK-ERK pathway in the treatment of cancer. Onkologie 25:511-8, 2002

28. Peyssonnaux C, Eychene A: The Raf/MEK/ERK pathway: new concepts of activation. Biol Cell 93:53-62, 2001

29. Giordano TJ, Kuick R, Thomas DG, et al: Molecular classification of papillary thyroid carcinoma: distinct BRAF, RAS, and RET/PTC mutation-specific gene expression profiles discovered by DNA microarray analysis. Oncogene 24:6646-56, 2005

30. Yoo SK, Lee S, Kim SJ, et al: Comprehensive Analysis of the Transcriptional and Mutational Landscape of Follicular and Papillary Thyroid Cancers. PLoS Genet 12:e1006239, 2016

31. Jones PA, Baylin SB: The epigenomics of cancer. Cell 128:683-92, 2007

32. Lee EK, Chung KW, Yang SK, et al: DNA methylation of MAPK signal-inhibiting genes in papillary thyroid carcinoma. Anticancer Res 33:4833-9, 2013

33. Rodriguez-Rodero S, Fernandez AF, Fernandez-Morera JL, et al: DNA methylation signatures identify biologically distinct thyroid cancer subtypes. J Clin Endocrinol Metab 98:2811-21, 2013

34. Cai LL, Liu GY, Tzeng CM: Genome-wide DNA methylation profiling and its involved molecular pathways from one individual with thyroid malignant/benign tumor and hyperplasia: A case report. Medicine (Baltimore) 95:e4695, 2016

35. Simarro M, Giannattasio G, De la Fuente MA, et al: Fas-activated serine/threonine phosphoprotein promotes immune-mediated pulmonary inflammation. J Immunol 184:5325-32, 2010

36. Ng EK, Shin VY, Leung CP, et al: Elevation of methylated DNA in KILLIN/PTEN in the plasma of patients with thyroid and/or breast cancer. Onco Targets Ther 7:2085-92, 2014

37. Sepulveda JL, Gutierrez-Pajares JL, Luna A, et al: High-definition CpG methylation of novel genes in gastric carcinogenesis identified by next-generation sequencing. Mod Pathol 29:182-93, 2016

38. Salati S, Zini R, Nuzzo S, et al: Integrative analysis of copy number and gene expression data suggests novel pathogenetic mechanisms in primary myelofibrosis. Int J Cancer 138:1657-69, 2016

39. Dohi O, Yasui K, Gen Y, et al: Epigenetic silencing of miR-335 and its host gene MEST in hepatocellular carcinoma. Int J Oncol 42:411-8, 2013

40. Vidal AC, Henry NM, Murphy SK, et al: PEG1/MEST and IGF2 DNA methylation in CIN and in cervical cancer. Clin Transl Oncol 16:266-72, 2014

41. Wang D, Cui W, Wu X, et al: RUNX3 site-specific hypermethylation predicts papillary thyroid cancer recurrence. Am J Cancer Res 4:725-37, 2014

42. Mitchell SM, Ross JP, Drew HR, et al: A panel of genes

methylated with high frequency in colorectal cancer. BMC Cancer 14:54, 2014

43. Loginov VI, Pronina IV, Burdennyi AM, et al: Role of Methylation in the Regulation of Apoptosis Genes APAF1, DAPK1, and BCL2 in Breast Cancer. Bull Exp Biol Med 162:797-800, 2017

44. Liu J, Li H, Sun L, et al: Aberrantly methylated-differentially expressed genes and pathways in colorectal cancer. Cancer Cell Int 17:75, 2017

45. Botezatu A, Iancu IV, Plesa A, et al: Methylation of tumour suppressor genes associated with thyroid cancer. Cancer Biomark 25:53-65, 2019

46. Ko HJ, Kim BY, Jung CH, et al: DNA methylation of RUNX3 in papillary thyroid cancer. Korean J Intern Med 27:407-10, 2012

47. Boot A, Oosting J, de Miranda NF, et al: Imprinted survival genes preclude loss of heterozygosity of chromosome 7 in cancer cells. J Pathol 240:72-83, 2016

48. Landa I, Pozdeyev N, Korch C, et al: Comprehensive Genetic Characterization of Human Thyroid Cancer Cell Lines: A Validated

Panel for Preclinical Studies. Clin Cancer Res 25:3141–3151, 2019

49. Schagdarsurengin U, Richter AM, Hornung J, et al: Frequent epigenetic inactivation of RASSF2 in thyroid cancer and functional consequences. Mol Cancer 9:264, 2010

50. Zhao H, Li J, Li X, et al: Silencing GPX3 Expression Promotes Tumor Metastasis in Human Thyroid Cancer. Curr Protein Pept Sci 16:316–21, 2015

51. Sanjari M, Kordestani Z, Safavi M, et al: Enhanced expression of Cyclin D1 and C–myc, a prognostic factor and possible mechanism for recurrence of papillary thyroid carcinoma. Sci Rep 10:5100, 2020

52. Zhang C, Bo C, Guo L, et al: BCL2 and hsa–miR–181a–5p are potential biomarkers associated with papillary thyroid cancer based on bioinformatics analysis. World J Surg Oncol 17:221, 2019

53. Fallahi P, Ruffilli I, Elia G, et al: Novel treatment options for anaplastic thyroid cancer. Expert Rev Endocrinol Metab 12:279–288, 2017

54. Sethi K, Sarkar S, Das S, et al: Biomarkers for the diagnosis of thyroid cancer. J Exp Ther Oncol 8:341–52, 2010

55. Gao H, Sun X, Wang H, et al: Long noncoding RNA SNHG22 increases ZEB1 expression via competitive binding with microRNA-429 to promote the malignant development of papillary thyroid cancer. Cell Cycle 19:1186-1199, 2020

56. Yan R, Yang T, Zhai H, et al: MicroRNA-150-5p affects cell proliferation, apoptosis, and EMT by regulation of the BRAF(V600E) mutation in papillary thyroid cancer cells. J Cell Biochem 119:8763-8772, 2018

57. Zhang Y, Liu G, Wu S, et al: Zinc finger E-box-binding homeobox 1: its clinical significance and functional role in human thyroid cancer. Onco Targets Ther 9:1303-10, 2016

58. Noreen F, Kung T, Tornillo L, Parker H, Silva M, Weis S, et al. DNA methylation instability by BRAF-mediated TET silencing and lifestyle-exposure divides colon cancer pathways. Clin Epigenetics. 2019 Dec;11(1):196.

59. Fang M, Ou J, Hutchinson L, Green MR. The BRAF oncoprotein functions through the transcriptional repressor MAFG to mediate the CpG Island Methylator phenotype. Mol Cell. 2014 Sep;55(6):904-15.

Acknowledgement

This study was published in the SCIE journal, Clinical and Experimental Otorhinolaryngology 2022; 15(3): 273-282. I would like to express my sincere gratitude to all my collaborators who helped me with this research (Seong Yun Ha, Hyeon-Gun Jee, Kwangsoo Kim, Su-jin Kim, Young Jun Chai, June Young Choi, and Kyu Eun Lee.)

국문 초록

갑상선 세포주에 유도된 *BRAF*^{V600E} 돌연변이에 의한 메틸화 변화

서울대학교 대학원

의학과 외과학 전공

이 진 욱

배경 및 목적: *BRAF*^{V600E} 돌연변이는 갑상선 유두암을 일으키는 주된 발암 변이이다. 본 연구의 목적은 갑상선 세포에 *BRAF*^{V600E} 돌연변이가 유도되었을 때 발생하는 DNA 메틸화와 유전자 발현 양상의 변화를 확인하는 것이다.

대상 및 방법: 연구자는 Nthy/ori 갑상선 세포주에 *BRAF* 유전자를 전사시켜 Nthy/BRAF 라는 세포주를 만들었고, *BRAF*^{V600E} 돌연변이가

있는 Nthy/V600E, *BRAF* 유전자에 돌연변이가 없는 Nthy/WT 로 구분하였다. Nthy/WT 와 Nthy/V600E 세포주별로 유전자 발현 마이크로어레이와 DNA 메틸화 어레이를 시행하였고, 두 타입의 데이터를 병합하여 DNA 메틸화와 유전자 발현이 역상관관계로 나타나는 유전자 부위를 탐색하였다. 어레이 분석 결과는 The Cancer Genome Atlas (TCGA) 데이터를 활용한 in-silico 방법과, 파이로서열분석 및 실시간 역전사 중합효소 연쇄반응 (qRT-PCR)을 통한 in-vivo 방법을 통해 검증하였다. .

결과: Nthy/V600E 세포주를 기준으로, 199,821 개의 프로브가 유의한 과메틸화를 보였으며, 697개의 유전자가 "과발현-유전자 발현 억제" 양상을 보였다. 이들 유전자군 중에는 종양 억제 유전자들과, 세포자멸사 관련 유전자들이 포함되었다. 66,446 개의 프로브는 유의한 저메틸화를 보였고, 227개의 유전자들이 "저메틸화-유전자 발현 증가" 양상을 보였다. 이들 유전자군 중에는 전암유전자와 단백질을 코딩하는 유전자들이 포함되었다. TCGA 검증에서, 491/697 (70.44%) 개의 유전자들이 동일한 "과메틸화-유전자 발현 억제" 양상을 보였으며, 153/227 (67.40%) 개의 유전자들이 동일한 "저메틸화-유전자 발현 증가" 양상을 보였다. 10개의 선택된 유전자들에서 파이로서열분석 및 qRT-PCR 결과가 마이크로어레이 결과와 유사한 양상을 보였다.

결론: 갑상선 세포에 유도된 *BRAF*^{V600E} 돌연변이는 더 많은 과메틸화 양상을 보였다. 종양 억제 유전자 및 세포자멸사 등의 항암 관련 유전자들이 과메틸화에 의해 발현이 억제되는 양상이 확인되었고, 전암유전자와 같은 발암 관련 유전자들이 저메틸화에 의해 발현이 증가되는 양상이 확인되었다. 본 연구의 결과는 *BRAF*^{V600E} 돌연변이가 DNA 메틸화 기전을 통해 종양과 관련된 유전자 발현을 조절할 수 있다는 것을 시사한다.

주요어: 갑상선 종양, DNA 메틸화, 유전자 발현

학 번: 2016-36691